Analysis of Multi-Resonance and Stability Enhancement Method in Multi-Source DC Distribution Power Systems

Yaoyao Zhang
School of Electrical Engineering
Southeast University
Nanjing, China
18351959765@163.com

Xiaohui Qu
School of Electrical Engineering
Southeast University
Nanjing, China
xhqu@seu.edu.cn

Fanlei Kong
School of Electrical Engineering
Southeast University
Nanjing, China
3375024578@qq.com

Gan Wang
School of Electrical Engineering
Southeast University
Nanjing, China
497079492@qq.com

***Abstract*—In multi-source distribution power systems (DPSs), line impedances of the source converter's output terminal will cause high-frequency oscillations, resulting in an unstable system. In this paper, the impedance-based analysis method is used to explain the reasons for instability at multiple frequency points in multi-source DPSs. The boundary conditions of cut-off frequencies of load converters and maximum resonance frequencies of the high-frequency resonance points are caused by line impedance and obtained through an impedance-based analysis method. For the unavoidable instability problems, this paper also investigates the parallel virtual impedance (PVI) methods of the load converter based on voltage-current double-loop control. The larger phase margin of the double-loop control scheme addresses the magnitude dip. Finally, the effectiveness of the above analysis is verified by experiment.**

Keywords—DC distribution power system, multiple source, line impedance, multiple resonances, stability enhancement

I. INTRODUCTION

With the introduction of renewable energy sources such as photovoltaic (PV) and wind power and the increase in DC loads, DC DPS has become mainstream [1]-[4]. The typical DC DPS consists of massive power electronic converters, including PV grid-connected units, energy storage units, load units, etc., as shown in Fig. 1. Due to the interaction between subsystems, even if the single converter is stable, the system still has instability problems [5]-[10].

For the complex DC DPS, some research based on the impedance ratio stability criterion have be carried out to make sure that the impedance ratio of Z_{oS}/Z_{inL} satisfies the Nyquist criterion, where Z_{oS} and Z_{inL} are the equivalent impedance of the source converter the load converter, respectively[11]-[12]. The existing active improvement methods based on impedance analysis can be classified into two types: active methods acting on the source side converter [13]-[15] and load side converter [16]-[18]. The active method of the source-side converter is to dampen the resonance peak of Z_{oS} to realize the total separation between $|Z_{oS}|$ and $|Z_{inL}|$. However, when the source converter is an uncontrollable system, such as an LC filter, these methods fail to improve system stability. Therefore, a virtual impedance is inserted in series into load converters to realize amplitude compensation for the whole system stability [17]. Another method is to compensate for the phase so that the phase difference $|\varphi(Z_{oS})-\varphi(Z_{inL})|$ is smaller than 180º without amplitude separation [16]-[18].

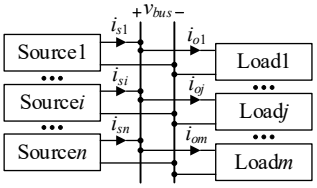

Fig. 1 A typical multi-source DC DPS.

However, the stability improvement method usually neglects the line impedance between converters and dc bus [19]. In the AC distribution system, the line impedance affects the resonance frequency directly with the inverter LCL filter [20]. In the DC DPS with multiple power electronic devices connected in parallel, the influence of line impedance is evident. References [21] and [22] study the influence of droop control and line impedance on DC microgrids based on the state-space method of characteristic root and sensitivity analysis, pointing out that line impedance and DC converter's output impedance interact with each other to trigger high-frequency oscillations. It is noted that multiple source converters connected in parallel will reduce damping and lead to oscillations. But high resonance frequencies and characteristics caused by line impedance are rarely proposed. Moreover, the magnitude dip of the load converter's input impedance will deteriorate system stability.

In response to the above issues, this paper investigates the multiple resonance peaks caused by line impedances. Firstly, a small-signal model of a multi-source DC DPS is established and expressions of three types of resonance frequencies are deduced. The boundary conditions for the instability problem caused by high-frequency resonances are obtained by analyzing the interaction between sources and loads. Furthermore, the boundary frequency at which the instability problem occurs is obtained, which is beneficial to the design of a cut-off frequency that can achieve stability enhancement at multiple resonance frequencies. Then, the effects of voltage loop control and voltage-current double-loop control on the magnitude dip of the load converter's input impedance are comparatively analyzed. Based on the PVI methods of the

This work was supported in part by the National Key Research and Development Program of China under Grant 2018YFB0904100, and in part by the Science and Technology Project of State Grid under Grant SGHB0000KXJS1800685.

double-loop control, the enhancement of the instability problem at multiple resonance frequencies is achieved. Finally, the validity of the analysis is verified by experiment.

II. Basic Analysis of Multiple Resonance and Design Criterion for Load Converters

A. Multiple Resonances

In Fig. 2, n source converters are connected in parallel to the dc bus, and multiple load converters connect in parallel to supply energy to the load, where Z_{oSi} (i = 1, 2,⋯, n) and Z_{inLj} (j = 1, 2,⋯, m) denote the ith source converter's output impedance and the jth load converter's input impedance, respectively, R_{li} and L_{li} are the line resistance and inductance separately. The output impedance of common DC/DC converters exhibits LC characteristics, so the source converters can be simplified as LC filters. Here, R_{fi}, L_{fi}, and C_{fi} are parasitic resistances, inductances, and capacitances, respectively. The load converters are controlled by PI controllers, where H_v is the sampling coefficient, G_v is the PI controller, G_m is the PWM generator, and R_L is the power load.

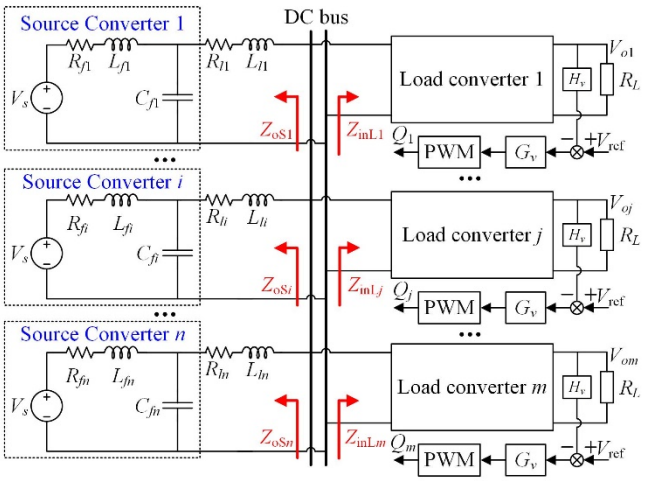

Fig. 2 A typical multi-source DC DPS.

The equivalent minor loop gain of multi-source DC DPS can be expressed as [11]

$$T_m(s)=\frac{Z_{oS}(s)}{Z_{inL}(s)}=\frac{\left(\sum_{i=1}^{n}1/Z_{oSi}(s)\right)^{-1}}{\left(\sum_{i=1}^{m}1/Z_{inLj}(s)\right)^{-1}} \tag{1}$$

where Z_{oS} is the shunt impedance of output impedances of source converters and Z_{inL} is the input impedance of load converter, respectively. The output impedance of the equivalent LC filter is

$$Z_{oSi}(s)=\frac{R_{fi}+L_{fi}s}{L_{fi}C_{fi}s^2+R_{fi}C_{fi}s+1}+R_{li}+L_{li}s \tag{2}$$

At the low-frequency range, the output impedance of the LC filter shows inductive characteristics, thus the line inductance L_{li} is much smaller than the inductance L_{fi} of the LC filter. From (2), it can be seen that each LC filter has a resonance frequency, and an inherent resonance frequency is formed by multiple LC filters connected in parallel as follows.

$$f_{r1}=\frac{1}{2\pi}\sqrt{\frac{\sum_{i=1}^{n}\left(\frac{1}{L_{fi}}\cdot\prod_{j=1}^{n}L_{fj}\right)}{\prod_{i=1}^{n}L_{fi}\cdot\sum_{i=1}^{n}C_{fi}}} \tag{3}$$

Then the magnitude peak of Z_{oS} corresponding to f_{r1} is

$$Z_{oS\_p1}=\frac{\prod_{i=1}^{n}L_{fi}\cdot\sum_{i=1}^{n}\left(\frac{1}{L_{fi}}\cdot\prod_{j=1}^{n}L_{fj}\right)}{\sum_{i=1}^{n}C_{fi}\cdot\sum_{i=1}^{n}\left(R_{fi}\cdot\prod_{j=1,j\neq i}^{n}L_{fj}^2\right)} \tag{4}$$

When the frequency is much than f_{r1}, i.e., in the high-frequency band, $\frac{1}{C_{fi}s}<<L_{fi}s+R_{fi}$. Considering the effect of line impedances and assuming that $L_{l1}<L_{l2}<\cdots<L_{ln}$ and $R_{l1}<R_{l2}<\cdots<R_{ln}$, the interaction between LC filters and line impedances leads to (n-1) high-frequency resonance frequency as follows.

$$f_{r2\_i}=\frac{1}{2\pi}\sqrt{\frac{C_{f(n-i)}+C_{f(n-i+1)}}{C_{f(n-i)}C_{f(n-i+1)}\left(L_{l(n-i)}+L_{l(n-i+1)}\right)}} \tag{5}$$

The corresponding magnitude peak of Z_{oS} is

$$Z_{oS\_p2\_i}=\frac{R_{l(n-i)}R_{l(n-i+1)}}{R_{l(n-i)}+R_{l(n-i+1)}}+\frac{\left(L_{l(n-i)}C_{f(n-i)}-L_{l(n-i+1)}C_{f(n-i+1)}\right)^2}{\left[C_{f(n-i)}C_{f(n-i+1)}\left(C_{f(n-i)}+C_{f(n-i+1)}\right)\cdot\left(R_{l(n-i)}+R_{l(n-i+1)}\right)\left(L_{l(n-i)}+L_{l(n-i+1)}\right)\right]} \tag{6}$$

According to (5), the main reason for the appearance of high-frequency resonance is that line inductances L_{li} resonates that the capacitances of LC filters.

Besides, the ith LC filter will cause resonance with its relevant line inductance L_{li} as follows.

$$f_{r3\_i}=\frac{1}{2\pi}\sqrt{\frac{L_{fi}+L_{li}}{L_{fi}L_{li}C_{fi}}} \tag{7}$$

The magnitude values in (7) are so tiny that they behave as the valley in the magnitude curve.

$$Z_{oS\_vi}=R_{li}\ \text{ at }\ f_{r3\_i} \tag{8}$$

From the above analysis, multiple resonance frequencies can be divided into three categories: the first is the inherent frequency of the LC filter; the second is the high-frequency caused by the line impedance and capacitance in the LC filter; the third is the resonance frequency caused by each LC filter and the corresponding line impedance, which presents a valley characteristic due to its small magnitude value.

B. Design Principle of Load Converter

The input impedance of the jth load converter with a single PI controller can be expressed as

$$Z_{inLj}(s)=\left[-\frac{T(s)}{1+T(s)}\cdot\frac{P_{oj}}{V_{bus}^2}+\frac{1}{1+T(s)}\cdot\frac{1}{Z_{in\_L}(s)}\right]^{-1} \tag{9}$$

where V_{bus} is the DC bus voltage and P_{oj} (j = 1, 2,⋯, m) is the load power. Here, $T(s) = H_vG_v(s)G_m(s)G_{vd\_L}(s)$ is the open-loop gain of the load converter with a voltage-loop controller. $G_{vd\_L}(s)$ is the open-loop transfer function of d to V_o. $Z_{in\_L}(s)$ is the open-loop input impedance.

It can be seen from (9) that $|T(s)|>>1$ at low frequencies and $|Z_{inLj}|$ can be simplified as V_{bus}^2/P_{oj}. The input impedance of m load converters connected in parallel is expressed as

$$Z_{inL} = -\frac{V_{bus}^2}{P_{o1} + P_{o2} + \cdots + P_{om}} = -\frac{V_{bus}^2}{P_o} \tag{10}$$

Thus, multiple load converters connected in parallel can be equated to one load converter to supply energy to the load.

In the low-frequency band, $|T(s)|$ is much larger than 1 and Z_{inL} can be simplified as V_{bus}^2/P_o. In the high-frequency band, $|T(s)|$ is much smaller than 1, and Z_{inL} is simplified as Z_{in_L}. The turning frequency is also the cut-off frequency f_c of the load converter [18].

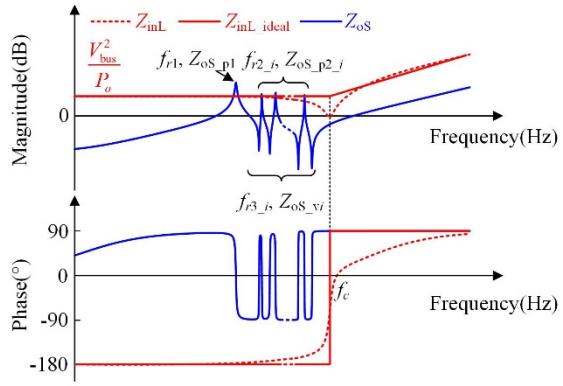

Fig.3 Bode plots of Z_{oS} and Z_{inL} with resonance frequencies.

The bode plots of Z_{oS} and Z_{inL} are depicted in Fig. 3. The magnitude of Z_{oS} has n resonance peaks and n resonance valleys. At the low-frequency band, the red line of Z_{inL} can be regarded as V_{bus}^2/P_o. According to the relationship between Z_{oS} and Z_{inL} in Fig. 3, the system stability can be determined as follows:

- If $Z_{oS\_p1} > V_{bus}^2/P_o$, the phase difference $|\varphi(Z_{oS})-\varphi(Z_{inL})|$ is greater than 180º, thus oscillation occur at the low-frequency f_{r1}.
- If $f_{r1} \le f_c \le f_{r2\_i}$, the magnitude of Z_{inL} increases linearly with frequency and is usually larger than $Z_{oS\_p2\_i}$. Even if Z_{inL} intersects with the magnitude of Z_{oS}, the phase difference $|\varphi(Z_{oS})-\varphi(Z_{inL})|$ is always smaller than 180º. Therefore, there is no high-frequency oscillation.
- If $f_c \ge f_{r2\_i}$, the system is stable provided that $V_{bus}^2/P_o > Z_{oS\_p1}$ and $V_{bus}^2/P_o > Z_{oS\_p2\_i}$. Otherwise, the bus voltage multiple frequency oscillation. Substituting (6) into $V_{bus}^2/P_o > Z_{oS\_p2\_i}$, f_{r2_i} for a stable system should be larger than the boundary f_{r2_ib}.

$$f_{r2\_i} > f_{r2\_ib} = \frac{1}{2\pi\sqrt{L_{l(n-i)}C_{f(n-i)} + \frac{1}{2}C_{f(n-i)}^2\Delta\left(1+\sqrt{1+\frac{4L_{l(n-i)}}{C_{f(n-i)}\Delta}}\right)}} \tag{11}$$

where $\Delta=(R_{l(n-i)}+R_{l(n-i+1)})V_{bus}^2/P_o - R_{l(n-i)}R_{l(n-i+1)}$.

It can be seen from Fig. 3 that there is a magnitude dip at f_c for Z_{inL}, which is likely to intersect with $|Z_{oS}|$ to generate new high-frequency oscillation. The voltage loop of the load converter is less effective at f_c, making it difficult to achieve further improvement. Besides, the influence of f_{r2_i} is unavoidable in some cases, f_c should be designed to be large enough to allow for stability improvements in the next section.

III. Parallel Virtual Impedance Method Based on Double-Loop Control Scheme

A. Double-Loop Control in Load Converter

From the above analysis, a comparative analysis of the single-loop and double-loop control is carried out to ensure that $f_c > f_{r2\_ib}$ and to eliminate magnitude dip. Then the stability margin of the load converter is very limited. $T(s)$ can be expressed as $1\angle(\varphi_m\text{-}180º)$ at f_c. When $T(s)<<1$, Z_{inL} can be equivalent to an inductance. Substituting $T(s)$ into (9), (12) can be obtained as follows.

$$|Z_{inL}(f_c)| = \left(\frac{\left(\frac{1}{Z_{in\_L}(f_c)}\right)^2 + \left(\frac{P_o}{V_{bus}^2}\right)^2}{4\sin^2\left(\frac{\varphi_m}{2}\right)} + \frac{1}{Z_{in\_L}(f_c)}\cdot\frac{P_o}{V_{bus}^2}\cdot\frac{1}{\tan\left(\frac{\varphi_m}{2}\right)}\right)^{-\frac{1}{2}} \tag{12}$$

As can be seen from (11), the magnitude dip of the load converter is mainly related to φ_m [23]-[24]. When φ_m=90º, $|Z_{inL}(f_c)| \approx V_{bus}^2/P_o$ and magnitude dip can be negligible. Fig. 4 shows the bode plots of $T(s)$ in (9) with different control parameters. As can be seen from Fig. 4, the cut-off frequency increases with the control parameter k_p increase, but the phase margin φ_m is close to 0. Therefore, it is difficult for a single voltage-loop controller to enhance f_c and suppress the magnitude dip.

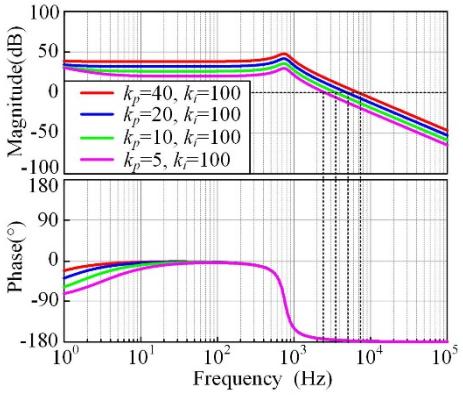

Fig. 4 Bode plots of $T(s)$ with different control parameters.

Therefore, a voltage-current double-loop controller with a greater phase margin is considered to suppress magnitude dip. A larger f_c and higher dynamic response are achieved by the inner current-loop controller of the double-loop control scheme. After using the double-loop control method, the input impedance Z_{inL}^D of the load converter is expressed as

$$Z_{inL}^D(s) = \left[-\frac{T'(s)}{1+T'(s)}\cdot\frac{P_o}{V_{bus}^2} + \frac{1}{1+T'(s)}\cdot\frac{1}{Z_{in\_L}}\right]^{-1} \tag{13}$$

where $T'(s) = T_v(s) + T_i(s)$. $T_v(s) = H_vG_v(s)G_i(s)G_m(s)G_{vd\_L}(s)$ is the outer voltage-loop gain and $T_i(s)=H_sG_i(s)G_m(s)G_{iLd\_L}(s)$ is the inner current-loop gain. Here, H_v and H_s are the

sampling coefficients, $G_i(s)$ is the current-loop PI controller, and $G_{iLd\_L}(s)$ is the transfer function of d to i_L. The bode plots of Z^{D}_{inL} and $T'(s)$ are shown in Fig. 5, where f_c increases much and φ_m is close to 90º. From Fig. 5, the magnitude dip at f_c is eliminated in the red magnitude line.

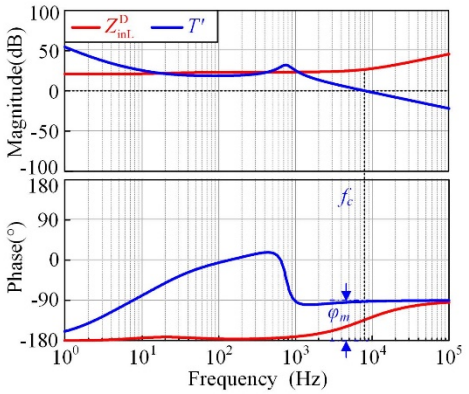

Fig. 5 Bode plots of Z^{D}_{inL} and $T'(s)$ with different control parameters.

B. Virtual Impedance Compensation

The virtual impedance control schemes based on double-loop control are similar to those based on voltage-loop control [18]. For improving the stability if there are multiple load converters, an effective method is to make $|\varphi(Z_{oS})-\varphi(Z^{D}_{inL})|$ within 180º by compensating the phase of Z^{D}_{inL}, which is called the parallel virtual impedance (PVI) method, as shown in Fig. 6. The perfect input impedance Z_{inL_P} of the load converter can be expressed as

$$Z_{inL\_P}(s)=\begin{cases}\left|Z^{D}_{inL}(s)\right|e^{j\theta_i}, & f\in[f_{i1},f_{i2}]\\ Z^{D}_{inL}(s), & f\notin[f_{i1},f_{i2}]\end{cases} \tag{14}$$

where f_{i1} and f_{i2} are the overlapping frequencies of Z_{oS} and Z^{D}_{inL}. θ_i is the phase angle value of the ideal load converter input impedance. To ensure that the phase difference is within 180º, $\theta_i \in$[-90º, 90º].

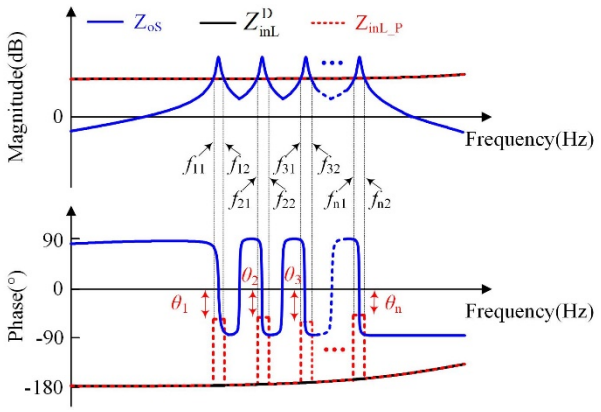

Fig.6 Phase compensation with PVI method.

Fig. 7 shows the control block diagram of the load converter with adding double-loop PVI feedback control, as shown in the blue solid line, where G_{ii_L} is the open-loop transfer function of i_o to i_{bus}, G_{id_L} is the open-loop transfer function of d_o to i_{bus}, G_{vv_L} is the open-loop transfer function of v_{bus} to v_o, G_{vd_L} is the open-loop transfer function of d_o to v_o, G_{iLv_L} is the open-loop transfer function of v_{bus} to i_{Lo}, G_{iLi_L} is the open-loop transfer function of i_o to i_{Lo}, and G_{iLd_L} is the open-loop transfer function of d_o to i_{Lo}. Z_{in_L} and Z_{o_L} are the open-loop input impedance and output impedance of the load converter, respectively. The PVI control delivers the bus voltage v_{bus} back into the output side of G_v. If one of the load converters uses the PVI method, the ideal load converter's input impedance with PVI control can be expressed as

$$\begin{aligned}Z_{inL\_P}(s)&=Z_{vir\_P}(s)\,\square\,Z^{D}_{inL1}(s)\,\square\cdots\square\,Z^{D}_{inLm}(s)\\&=\frac{Z^{D}_{inL\_P}Z_{vir\_P}(s)}{Z^{D}_{inL\_P}+Z_{vir\_P}(s)}\end{aligned} \tag{15}$$

where $Z^{D}_{inL\_P}(s)= Z^{D}_{inL1}(s)\|\cdots\|Z^{D}_{inLm}(s)$.

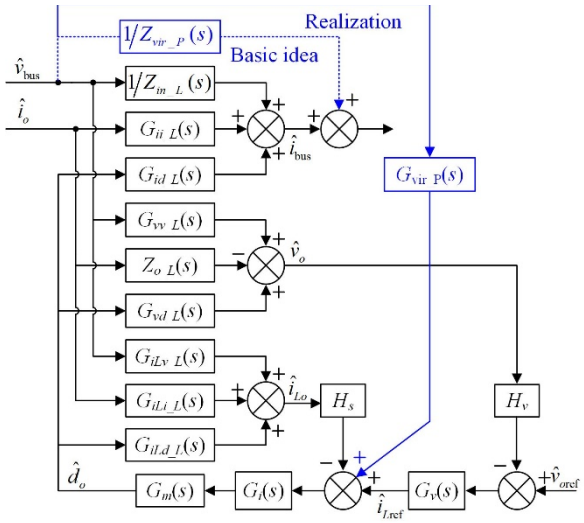

Fig. 7 Control block diagram of the load converter with PVI control strategy.

Substituting (14) into (13), we have

$$Z_{vir\_P}=\frac{1}{\dfrac{1}{Z_{inL\_P}}-\dfrac{1}{Z^{D}_{inL\_P}}}=\begin{cases}\dfrac{\left|Z^{D}_{inL\_P}\right|}{1+e^{-j\theta_i}}, & f\in[f_{i1},f_{i2}]\\ +\infty, & f\notin[f_{i1},f_{i2}]\end{cases} \tag{16}$$

Therefore, to obtain a smooth transfer function, (16) can be further expressed as

$$\begin{aligned}G_{vir\_P}(s)=&\frac{1+T_v(s)+T_i(s)}{G_i(s)G_m(s)G_{id\_L}(s)}\cdot\\&\left[\frac{1+e^{-j\theta_1}}{\left|Z^{D}_{inL\_P}(s)\right|}G_{BPF1}(s)+\cdots+\frac{1+e^{-j\theta_n}}{\left|Z^{D}_{inL\_P}(s)\right|}G_{BPFn}(s)\right]\end{aligned} \tag{17}$$

where $G_{BPFi}(s)$ are bandpass filters.

IV. Simulation and Experimental Verifications

TABLE I. Simulation and Experimental Parameters

Parameter	Value
bus vlotage V_{bus}	48 V
source filter $R_{f1,2}/L_{f1,2}$, $C_{f1,2}$	0.1 Ω/1200 μH, 100 μF
line resistor R_{l1}, R_{l2}	0, 0.02 Ω
line inductor L_{l1}, L_{l2}	0, 180 μH
load output voltage V_o	24 V
load filter L_o, C_o	200 μH, 220 μF
voltage PI parameter k_p, k_i	0.5, 100
current PI parameter k_{pi}, k_{ii}	5, 100
output power P_o	200W

The instability problem is more obvious when the source converter is an LC filter. Therefore, two LC filters are used as source converters connected to the dc bus to supply the load

via the buck converter. The system parameters in the simulation and experiment are given in Table 1. Therefore, there are two resonance peaks at f_{r1} of 459 Hz and f_{r2_1} of 1678 Hz by (3) and (5). The resonance valley is located at f_{r3_1} of 1272Hz by (7).

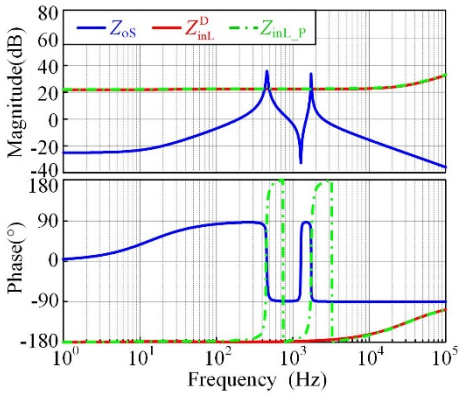

Fig. 8 Bode plots of Z_{oS}, Z^{D}_{inL}, and Z_{inL_P}.

Fig. 8 shows the bode plot of the input impedance of the load converter with the PVI strategy, where Z_{oS} overlaps with Z^{D}_{inL} at the calculated values of 459Hz and 1678 Hz. The phase difference between Z_{oS} and Z^{D}_{inL} is larger than 180º, which indicates that the system has two oscillation frequency points. Meanwhile, the double-loop control scheme has a cut-off frequency, which facilitates stability improvement at a high resonance frequency range. The PVI control method (green dashed line) compensates for the phase of Z^{D}_{inL} at the unstable resonance points. It can be seen from Fig. 8 that the phase difference is smaller than 180º in the overlapping range.

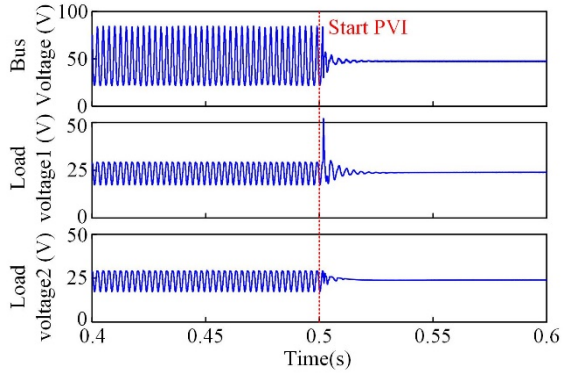

Fig. 9 Simulation waveforms in the system with a load converter using PVI.

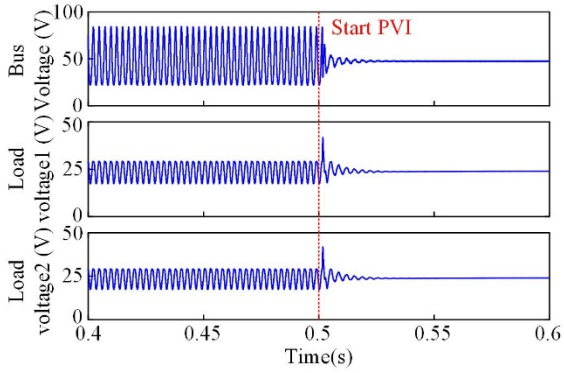

Fig. 10 Simulation waveforms in the system with two load converters using PVI.

Figs. 9 and 10 show the simulation waveforms of DC DPS composing an LC filter and two load converters. When a load converter uses a PVI control strategy and another does not, the simulation waveforms of bus voltage V_{bus}, load voltage V_{o1}, and load voltage V_{o2} as shown in Fig. 9. Fig. 10 illustrates the simulation waveforms of bus voltage V_{bus} and load voltage $V_{o1,2}$ with two 100W load converters using PVI control strategies. As seen in Fig. 9 and 10, the two systems are unstable before 0.5s. After starting the PVI control strategy, the oscillations in Fig. 9 and 10 are eliminated within several oscillation periods. Therefore, connecting PVI in parallel to a single load converter has the same effect as connecting PVIs in parallel to multiple load converters. To facilitate the design, the multiple load converters can be regarded as a load converter in the experiment.

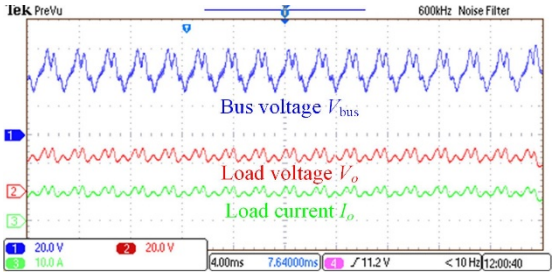

Fig. 11 Experimental waveforms of bus voltage V_{bus}, load voltage V_o, and load current I_o.

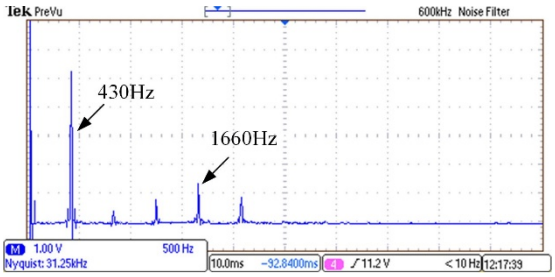

Fig. 12 Fourier analysis of V_{bus}.

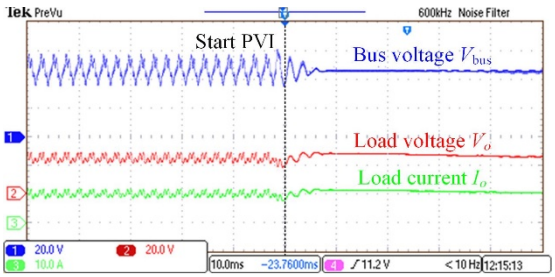

Fig. 13 Experimental waveforms of the load converter with PVI method.

The experimental waveforms V_{bus}, V_o, and I_o are given in Fig. 11. It is apparent from Fig. 10 that the bus voltage has two oscillation frequencies. A Fourier analysis of the bus voltage V_{bus} is shown in Fig. 12, from which it can be seen that two oscillation frequencies of 430 Hz and 1660 Hz, consistent with the results in Fig. 8. To verify the effect of the PVI method, Fig. 13 gives the experimental waveforms of V_{bus}, V_o, and I_o without virtual impedance and with the PVI method. After the PVI method is inserted, the oscillations of V_{bus}, V_o, and I_o are manifestly suppressed. The system becomes stable which coincides with the theoretical analysis in Section III.

V. Conclusion

In this paper, resonance problems caused by line impedance in multi-source DC distribution power systems are

discussed and its small-signal impedance model is established. The influence of line impedance on the high-frequency resonance is analyzed to obtain the boundary conditions and maximum resonance frequency for the instability problem of multiple resonance peaks. A reasonable cut-off frequency is designed depending on the relationship between the load converter's cut-off frequency and the maximum resonance frequency. The load converter is controlled by a double-loop controller to obtain a reasonable cut-off frequency and to avoid magnitude dip. Using the PVI method based on the double-loop control to improve the system stability, the PVI control method on a single load converter can effectively suppress the system instability problem. Finally, simulation and experimental results verify the effectiveness and feasibility of the above analysis and method.

REFERENCES

[1] R. Haroun, A. Cid-Pastor, A. E. Aroudi, and L. Martlnez-Salamero, "Synthesis of canonical elements for power processing in DC distribution systems using cascaded converters and sliding-mode control," *IEEE Trans. Power Electron.*, vol. 29, no. 3, pp. 1366-1381, Mar. 2014.

[2] T. Dragičević, X. Lu, J. C. Vasquez, and J. M. Guerrero, "DC microgrids—Part I: A review of control strategies and stabilization techniques," *IEEE Trans. Power Electron.*, vol. 31, no. 7, pp. 4876-4891, Jul. 2016.

[3] A. M. Colak and O. Kaplan, "A review on the efficiency increment in a power system using smart grid technologies," in *9th Int. Conf. Smart Grid, icSmartGrid* 2021, pp. 192-196, 2021.

[4] D. Icaza, J. R. Espinoza, and D. Valarezo, "Scenarios of operation of an energy production system of a hybrid WT/PV system of a bioecological infrastructure," in *9th Int. Conf. Smart Grid, icSmartGrid* 2021, pp. 306-311, 2021.

[5] Z. Jin, L. Meng, J. M. Guerrero, and R. Han, "Hierarchical control design for a shipboard power system with DC distribution and energy storage aboard future more-electric ships," *IEEE Trans. Ind. Inf.*, vol. 14, no. 2, pp. 703-714, Feb. 2018.

[6] O. Henni and M. Belarbi, "Effect of mathematical models on forecasting analysis of photovoltaic power," in *9th Int. Conf. Smart Grid, icSmartGrid* 2021, pp. 163-166, 2021.

[7] K. Strunz, E. Abbasi, and D. N. Huu, "DC microgrid for wind and solar power integration," *IEEE J. Emerg. Sel. Topics Power Electron.*, vol. 2, no. 1, pp. 115-126, Mar. 2014.

[8] F. Ayadi, I. Colak, I. Garip, and H. I. Bulbul, "Impacts of renewable energy resources in smart grid," in *8th Int. Conf. Smart Grid, icSmartGrid* 2020, pp. 183-188, 2020.

[9] S. M. S. Hosseinimoghadam, H. Roghanian, M. Dashtdar, and S. M. Razavi, "Power-sharing control in an islanded microgrid using virtual impedance," in *8th Int. Conf. Smart Grid, icSmartGrid* 2020, pp. 73-77, 2020.

[10] M. Su, Z. Liu, Y. Sun, H. Han, and X. Hou, "Stability analysis and stabilization methods of DC microgrid with multiple parallel-connected DC-DC converters loaded by CPLs," *IEEE Trans. Smart Grid*, vol. 9, no. 1, pp. 132-142, Jan. 2018.

[11] X. Zhang, X. Ruan, and C. K. Tse, "Impedance-based local stability criterion for DC distributed power systems," *IEEE Trans. Circuits Syst. I*, Reg. Papers, vol. 62, no. 3, pp. 916-925, Mar. 2015.

[12] R. D. Middlebrook, "Input filter considerations in design and application of switching regulators," in *Proc. IEEE IAS*, 1976, pp. 366-382.

[13] A. M. Rahimi and A. Emadi, "Active damping in DC/DC power electronic converters: A novel method to overcome the problems of constant power loads," *IEEE Trans. Ind. Electron.*, vol. 56, no. 5, pp. 1428-1439, May 2009.

[14] M. Wu and D. D. Lu, "A novel stabilization method of LC input filter with constant power loads without load performance compromise in DC microgrids," *IEEE Trans. Ind. Electron.*, vol. 62, no. 7, pp. 4552-4562, Jul. 2015.

[15] A. Aldhaheri and A. H. Etemadi, "Stabilization and performance preservation of DC-DC cascaded systems by diminishing output impedance magnitude," *IEEE Trans. Ind. Appl.*, vol. 54, no. 2, pp. 1481-1489, Mar./Apr. 2018.

[16] M. N. Hussain and V. Agarwal, "A novel feedforward stabilizing technique to damp power oscillations caused by DC-DC converters fed from a DC bus," *IEEE J. Emerg. Sel. Topics Power Electron.*, vol. 8, no. 2, pp. 1528-1535, Jun. 2020.

[17] X. Zhang, X. Ruan, and Q. C. Zhong, "Improving the stability of cascaded DC/DC converter systems via shaping the input impedance of the load converter with a parallel or series virtual impedance," *IEEE Trans. Ind. Electron.*, vol. 62, no. 12, pp. 7499-7512, Dec. 2015.

[18] X. Zhang, Q. C. Zhong, and W. Ming, "Stabilization of cascaded DC/DC converters via adaptive series-virtual-impedance control of the load converter," *IEEE Trans. Power Electron.*, vol. 31, no. 9, pp. 6057-6063, Sept. 2016.

[19] Y. Li, Z. Shuai, X. Liu, Y. Chen, Z. Li, Y.Hong, and Z. J. Shen, "Stability analysis and location optimization method for multiconverter power systems based on nodal admittance matrix," *IEEE J. Emerg. Sel. Topics Power Electron.*, vol. 9, no. 1, pp. 529-538, Feb. 2021.

[20] J. He, Y. W. Li, D. Bosnjak, and B. Harris, "Investigation and active damping of multiple resonances in a parallel-inverter-based microgrid," *IEEE Trans. Power Electron.*, vol. 28, no. 1, pp. 234-246, Jan. 2013.

[21] L. Guo, S. Zhang, X. Li, Y. W. Li, C. Wang, and Y. Feng, "Stability analysis and damping enhancement based on frequency-dependent virtual impedance for DC microgrids," *IEEE J. Emerg. Sel. Topics Power Electron.*, vol. 5, no. 1, pp. 338-350, Mar. 2017.

[22] N. Rashidirad, M. Hamzeh, K. Sheshyekani, and E. Afjei, "High-frequency oscillations and their leading causes in DC microgrids," *IEEE Trans. Energy Convers.*, vol. 32, no. 4, pp. 1479-1491, Dec. 2017.

[23] J. Zhang, X. Xie, D. Jiao, and Z. Qian, "Stability problems and input impedance improvement for cascaded power electronic systems," in *Proc. IEEE Appl. Power Electron. Conf. Expo.*, pp. 1018-1024, 2004.

[24] Y. Zhang, X. Qu, G. Wang, W. Chen and Z. Huang, "Investigation of multiple resonances and stability enhancement in multi-source DC distribution power systems," *IEEE J. Emerg. Sel. Topics Circuits Syst.*, tovol. 12, no. 1, pp. 90-97, Mar. 2022.